Environmental Science Processes & Impacts

PAPER

Cite this: *Environ. Sci.: Processes Impacts*, 2017, **19**, 288

Quantifying the equilibrium partitioning of substituted polycyclic aromatic hydrocarbons in aerosols and clouds using COSMOtherm†

Boluwatife Awonaike,[a] Chen Wang,[a] Kai-Uwe Goss[b] and Frank Wania*[a]

Received 26th November 2016
Accepted 16th January 2017

DOI: 10.1039/c6em00636a

rsc.li/process-impacts

Functional groups attached to polycyclic aromatic hydrocarbons (PAHs) can significantly modify the environmental fate of the parent compound. Equilibrium partition coefficients, which are essential for describing the environmental phase distribution of a compound, are largely unavailable for substituted PAHs (SPAHs). Here, COSMOtherm, a software based on quantum-chemical calculations is used to estimate the atmospherically relevant partition coefficients between the gas phase, the aqueous bulk phase, the water surface and the water insoluble organic matter phase, as well as the salting-out coefficients, for naphthalene, anthracene, phenanthrene, benz(*a*)anthracene, benzo(*a*)pyrene and dibenz(*a*,*h*)anthracene and 62 of their substituted counterparts. They serve as input parameters for the calculation of equilibrium phase distribution of these compounds in aerosols and clouds. Our results, which were compared with available experimental data, show that the effect of salts, the adsorption to the water surface and the dissolution in a bulk aqueous phase can be safely neglected when estimating the gas–particle partitioning of SPAHs in aerosols. However, for small PAHs with more than one polar functional group the aqueous phase can be the dominant reservoir in a cloud.

Environmental impact

Substituted PAHs elicit interest because of their toxicity and their ability to absorb UV-VIS radiation. The potential health effects and the radiative properties of SPAHs depend on their distribution between the gas and particle phases in the atmosphere. Empirical information on this phase distribution is very limited, as are data on compound volatility typically used to estimate it. Here we show that software based on quantum-chemistry can estimate their atmospheric phase distribution behavior from molecular structure alone.

1 Introduction

Polycyclic aromatic hydrocarbons (PAHs) are a ubiquitous group of environmental contaminants which have been widely studied; some are known to be carcinogenic.[1] While parent PAHs have been studied extensively, much less is known about the substituted PAHs (SPAHs), which include alkyl-, keto-, oxo-, amino-, nitro-, cyano-PAHs, and heterocyclic aromatic compounds.[2] SPAHs, particularly those with alkyl substituents, are abundant in the atmospheric environment, formed and released primarily from the incomplete combustion of carbon-based materials.[3] Other sources include natural sources and atmospheric reactions of parent PAHs.[3] SPAHs have been shown to be just as toxic and sometimes even more toxic than their parent compounds.[4–6] Furthermore, due to their ability to absorb light in the UV-VIS range, SPAHs are suspected to contribute to the radiative properties of atmospheric 'brown carbon' (*e.g.* Fig. S8† in Lin *et al.*[7]). In order to (i) assess the extent to which humans are exposed to these compounds and the possible risks involved and (ii) understand the radiative properties of aerosols and clouds, it is important to understand the behavior of these compounds in the environment, especially in the atmosphere.

The transport and removal behavior of a chemical[8] and its reactive fate[9,10] in the atmosphere depend strongly on its distribution between the gas and particle phases. For example, Zhou *et al.*[10] showed that depending on the particle properties and ambient conditions, the reactivity of compounds adsorbed to particles could be significantly retarded, thus escalating their persistence and long-range transport. Furthermore, the extent to which these compounds pose risks to humans *via* inhalation depends on their gas–particle distribution.[11] Gaseous phase contaminants are more likely to be inhaled, while droplet-bound contaminants will be more susceptible to deposition within the airways. Finally, the gas–

---

[a] *Department of Physical and Environmental Sciences, University of Toronto Scarborough, 1265 Military Trail, Toronto, Ontario, M1C, 1A4, Canada. E-mail: frank.wania@utoronto.ca*

[b] *Department of Analytical Environmental Chemistry, Helmholtz Centre for Environmental Research GmbH – UFZ, Permoserstraße 15, 04318 Leipzig, Germany*

† Electronic supplementary information (ESI) available. See DOI: 10.1039/c6em00636a

particle distribution of chromophoric molecules has implications for the absorptive properties of aerosols.

It is thus important to understand the gas–particle partitioning behavior of the SPAHs. This distribution is influenced by a number of factors, including particle size and composition, temperature, relative humidity and the properties of the chemical.[12–14] The gas–particle partitioning behavior has been experimentally determined for parent PAHs,[14–16] and more recently and to a lesser extent, also for some SPAHs, particularly nitro-, oxo- and alkyl-PAHs.[3,17,18] However, considering the large number of SPAHs in existence, along with their diverse properties, the number of measurements is presently insufficient and unlikely to greatly expand in the near future. It is thus relevant that various prediction methods have been developed for the purpose of estimating gas–particle partitioning. These include the Junge–Pankow adsorption model,[19] the dual black carbon (soot) adsorption and organic matter absorption model,[20] and the empirical organic matter absorption relationships, which are based on the octanol–air partitioning coefficient ($K_{O/G}$) (*e.g.* Finizio *et al.*[21]). All these methods have been applied to estimate the gas–particle partitioning of SPAHs, particularly nitro- and oxy-PAHs. However, there have been multiple reports of underestimations,[11,17,18] and in some cases, overestimations.[11]

Characterizing the atmospheric phase partitioning of SPAHs (and PAHs) is potentially quite complex as it involves (i) likely (at least) two bulk phases (an organic phase and an aqueous phase), (ii) possibly bulk phase partitioning (absorption) and surface adsorption,[22] and (iii) in the case of aerosol, the need to account for the effect of salt on aqueous phase partitioning.[23] In other words, the prediction of atmospheric phase partitioning really involves the prediction of multiple distribution equilibria and of the Setschenow coefficient (K_S). In Fig. 1, which shows these processes and associated parameters, it is theorized that a chemical will partition to the different phases in these particles (aerosols and cloud droplets), with each phase contributing to the overall gas–particle distribution. We assume that the particle separates into a mostly aqueous phase and a water insoluble organic matter (WIOM) phase, which is mostly made up of organic compounds.[24–27] We also make the assumption that the particles are in the liquid form and PAHs and SPAHs achieve equilibrium partitioning instantaneously. In reality, particles may on occasion be semi-solids or solids (*i.e.* more viscous), which could slow down the exchange processes.[28] In that case, the kinetics of uptake and loss need to be taken into account.[10,29]

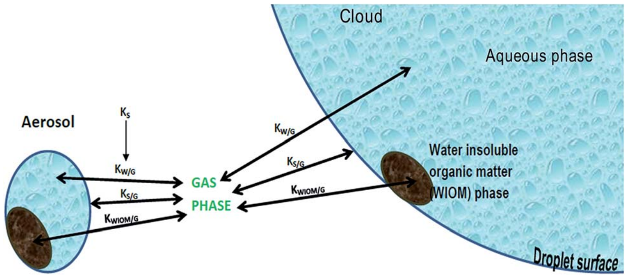

Fig. 1 Conceptual diagram of the partitioning of an organic compound between the gas phase and an aerosol (left) or cloud droplet (right). In either case, the droplets are assumed to separate into a (possibly salty) aqueous phase and a water insoluble organic matter (WIOM) phase. Quantification of partitioning in these systems requires three equilibrium partition coefficients (between the bulk aqueous phase and gas $K_{W/G}$; between the water droplet surface and gas $K_{S/G}$ and between WIOM and gas $K_{WIOM/G}$) and the Setschenow coefficient K_S.

The equilibrium partition coefficients included describe the distribution of chemicals between the bulk aqueous phase and gas ($K_{W/G}$), the droplet surface and the gas ($K_{S/G}$) and the WIOM and the gas ($K_{WIOM/G}$). K_S accounts for the effects of inorganic salts on the phase partitioning in aerosol particles.

Earlier approaches to estimating gas–particle partitioning of SPAHs have made simplifying assumptions (*e.g.* consider only one bulk phase, consider only bulk phase partitioning, but not surface sorption or *vice versa*, disregard the salting-out effect).[11,18,30] While these simplifications may be justified, this should be ascertained. Very few approaches exist that would allow for the prediction of all of the relevant *K*-values. While this is possible with poly-parameter linear free energy relationships (ppLFERs),[31] this requires the assumption that SPAHs fall within the applicability domain of those relationships. Recently, COSMOtherm has been used to predict partitioning of organic substances into aerosol bulk phases[32,33] and to predict Setschenow coefficients.[23] Wang *et al.*[35] have shown how these predictions can be combined to estimate gas–particle partitioning of compounds implicated in secondary organic aerosol formation, while disregarding surface adsorption. In the case of PAHs and SPAHs (*i.e.* flat molecules that can be quite large) it may not be justified to neglect the contribution of surface adsorption. Goss[37] has previously shown that COSMOtherm can also be used to estimate adsorption ($K_{S/G}$).

Here we combine different COSMOtherm-predicted *K*-values to assess the gas–particle partitioning of SPAHs. It serves as an illustration of how the gas–particle partitioning of organic chemicals can be assessed comprehensively with a quantum-chemical based approach if only their molecular structure is known. It also allows for the assessment of the validity of different simplifying assumptions made in the estimation of gas–particle partitioning. Finally, it allows us to explore how substitution with different types and numbers of functional groups affects the gas–particle partitioning of PAHs.

2 Methods

2.1 Calculating phase distribution

The fraction of the total amount of an atmospheric chemical present in each of four phases (gas phase, aqueous phase, water insoluble organic matter (WIOM) phase and water surface) can be calculated from the following equations (from Lei and Wania[38] modified to fit a four-phase system):

$$\Phi_G = \frac{1}{1 + \dfrac{V_W K_{W/G}}{V_G} + \dfrac{A}{V_G K_{G/S}} + \dfrac{V_{WIOM} K_{WIOM/G}}{V_G}} \tag{1}$$

$$\Phi_{\mathrm{W}} = \frac{1}{1 + \frac{A}{V_{\mathrm{W}} K_{\mathrm{W/G}} K_{\mathrm{G/S}}} + \frac{V_{\mathrm{WIOM}} K_{\mathrm{WIOM/G}}}{V_{\mathrm{W}} K_{\mathrm{W/G}}} + \frac{V_{\mathrm{G}}}{V_{\mathrm{W}} K_{\mathrm{W/G}}}} \quad (2)$$

$$\Phi_{\mathrm{S}} = \frac{1}{1 + \frac{V_{\mathrm{W}} K_{\mathrm{W/G}} K_{\mathrm{G/S}}}{A} + \frac{V_{\mathrm{WIOM}} K_{\mathrm{WIOM/G}} K_{\mathrm{G/S}}}{A} + \frac{V_{\mathrm{G}} K_{\mathrm{G/S}}}{A}} \quad (3)$$

$$\Phi_{\mathrm{WIOM}} = \frac{1}{1 + \frac{V_{\mathrm{W}} K_{\mathrm{W/G}}}{V_{\mathrm{WIOM}} K_{\mathrm{WIOM/G}}} + \frac{A}{V_{\mathrm{WIOM}} K_{\mathrm{WIOM/G}} K_{\mathrm{G/S}}} + \frac{V_{\mathrm{G}}}{V_{\mathrm{WIOM}} K_{\mathrm{WIOM/G}}}} \quad (4)$$

where Φ_{G}, Φ_{W}, Φ_{S} and Φ_{WIOM} are the fractions of the chemical present in the gas phase, bulk water (aqueous) phase, water surface and WIOM phase, respectively. V_{W}, V_{G} and V_{WIOM} represent the volumes (m^3) of the aqueous, gas and WIOM phases, A is the total surface area of the droplets (m^2) and K represents the various partition coefficients as described above. Table 1 shows the values used and assumptions employed in the calculation of phase distribution.

The total surface area (A) of aerosols and cloud droplets was calculated using the assumed radii in Table 1 and the equation for the total surface area of a sphere. The selected OAL of 10 μg m^{-3} is the average of the range of 0.1 to 20 μg m^{-3} reported as typical for the atmosphere.[40]

The salting out effect is defined by the following equation:[41]

$$\log(K_{1/\mathrm{saltwater}}/K_{1/\mathrm{water}}) = K_{\mathrm{S}}[\mathrm{salt}] \quad (5)$$

where $K_{1/\mathrm{saltwater}}$ and $K_{1/\mathrm{water}}$ are equilibrium partitioning coefficients of an organic solute between the aqueous phase and another non-aqueous phase, [salt] (mol L^{-1}) is the salt concentration, and K_{S} (M^{-1}) is the Setschenow coefficient which depends on the type of organic solute as well as on the type of salt.[42] For aerosol particles, the partition coefficient between the aqueous and gas phases is corrected for the salting out effect using this equation from Wang *et al.*[23]

$$\log K_{\mathrm{W/G,corrected}} = \log K_{\mathrm{W/G}} - K_{\mathrm{S}}[\mathrm{salt}] \quad (6)$$

This corrected $\log K_{\mathrm{W/G}}$ value is used in all calculations involving aerosols.

2.2 Predicting partition coefficients

All required partition coefficients $K_{\mathrm{W/G}}$, $K_{\mathrm{S/G}}$, $K_{\mathrm{WIOM/G}}$ and K_{S} are predicted at 25 °C using COSMOtherm, a software which predicts solvation equilibria from molecular structure alone.[43] COSMOtherm calculates solvation mixture thermodynamics based on quantum chemistry using COSMO-RS theory.[44,45] COSMO-RS combines an electrostatic theory of locally interacting molecular surface descriptors with an exact statistical thermodynamics methodology to obtain partition coefficients and other properties such as salting out coefficients.[44] In this approach, Simplified Molecular-Input Line-Entry System (SMILES) strings for the compounds of interest were generated from their molecular structures using the University of Cambridge OPSIN Tool.[46] Open Babel[47] was used to convert SMILES strings to spatial data files (.sdf) which serve as input data to COSMOconf (v. 3.0, COSMOlogic GmbH & Co. KG, Leverkusen, Germany, 2014). COSMOconf searches for the lowest energy conformers of the compounds in the gas phase, optimized with TURBOMOLE (v. 4.1.1, COSMOlogic GmbH & Co. KG, Leverkusen, Germany, 2015), and generates COSMO-files. Up to 10 of the lowest energy COSMOfiles are then fed into COSMOtherm (version C30_1601 with BP_TZVPD_FINE_C30_1601 parameterization, COSMOlogic GmbH & Co. KG, Leverkusen, Germany, 2016) to calculate $K_{\mathrm{W/G}}$, $K_{\mathrm{S/G}}$, $K_{\mathrm{WIOM/G}}$ and K_{S} at 25 °C. For purposes of comparison with measured data, we also calculated these coefficients at other temperatures (19.5 °C, 11.23 °C and 13.64 °C) (Table S4†). This simply involves changing the temperature in the COSMOtherm software after the COSMO-files have been input.

The prediction of $K_{\mathrm{WIOM/G}}$ using COSMOtherm is described in Arp and Goss.[32] Both coefficients $K_{\mathrm{W/G}}$ and $K_{\mathrm{WIOM/G}}$ are estimated similarly using the Henry's law constant property in COSMOtherm, with the condensed phase being water for $K_{\mathrm{W/G}}$, and for $K_{\mathrm{WIOM/G}}$, a non-polar, hypothetical structure 'B' (Fig. S6†). K_{S} for 6.6 M ammonium sulfate solution[35,36] was calculated according to Wang *et al.*[23] Briefly, partition coefficients between the gas phase and pure water, and between the gas phase and ammonium sulfate solution (salt water) were calculated using COSMOtherm. Using the relationships in

Table 1 Parameters and assumptions for estimation of phase distribution

Parameters	Value	Assumption	Reference
Organic aerosol loading (OAL)	10 μg WIOM per m^3 of air ($V_{\mathrm{WIOM}}/V_{\mathrm{G}} = 10^{-11}\ \mathrm{m}^3\ \mathrm{m}^{-3}$)	Density of WIOM = 10^6 g m^{-3}	33
Liquid water content (LWC)	Cloud: 0.3 g of water per m^3 of air ($V_{\mathrm{W}}/V_{\mathrm{G}} = 3 \times 10^{-7}\ \mathrm{m}^3\ \mathrm{m}^{-3}$)		33
	Aerosol: 10 μg of water per m^3 of air ($V_{\mathrm{W}}/V_{\mathrm{G}} = 10^{-11}\ \mathrm{m}^3\ \mathrm{m}^{-3}$)		33
Salt concentration	Cloud: 0 M	Salts are too diluted to result in significant salting out	34
	Aerosol: 6.6 M ammonium sulfate	Aerosol at 60% relative humidity	35, 36
Radius	Cloud: 1 mm or 0.1 mm	Perfect sphere	38
	Aerosol: 1 μm or 0.1 μm	Perfect sphere	39

eqn (5) and (6), these values were combined to estimate the Setschenow coefficient and to correct for the effects of ammonium sulfate on partitioning in aerosols. Because COSMOtherm has previously been shown to overestimate K_S,[23] the predicted K_S were corrected using the equation $K_S = 0.334K_{S,COSMOtherm} + 0.0604$.[23] $K_{S/G}$ was calculated based on the method described in Goss.[37] The Henry's law constant property was used to estimate the vacuum/gas partitioning coefficients ($K_{V/G}$) for the target compounds by simply setting vacuum as the pure phase. Next, the surface/vacuum partitioning coefficients ($K_{S/V}$) for the compounds were estimated using the Flatsurf partitioning property in COSMOtherm. For accurate results, it is essential to set the vacuum as phase 1 and the water surface as phase 2. $K_{V/G}$ and $K_{S/V}$ were then combined by applying a thermodynamic cycle, yielding $K_{S/G}$.

These coefficients were estimated for a total of 68 compounds – naphthalene, anthracene, phenanthrene, benz(*a*)anthracene, benzo(*a*)pyrene, dibenz(*a*,*h*)anthracene and 62 of their substituted counterparts. The substituents considered include: alkyl, nitro, hydroxyl, azaarene and dione. Isomers are also included in this study to investigate the effect of structure and substituent position on phase partitioning. A list of all the target compounds is given in Table S1 in the ESI.†

2.3 Evaluation of model predictions

For a limited number of compounds, the partition coefficients predicted by COSMOtherm could be compared with experimental data from the literature. While measured $K_{W/G}$ values are most frequently reported,[48,49] data are primarily available for parent PAHs and alkyl-naphthalenes. Only for naphthalene have $K_{S/G}$ and K_S been measured,[50,51] while experimental $K_{WIOM/G}$ values are not available for any of the compounds considered. Predicted $K_{WIOM/G}$ values were therefore compared with measured octanol–air partitioning coefficients $K_{O/G}$,[48,49] which have also been used to describe gas–particle partitioning.[21,52] For evaluation, we also compared COSMOtherm-calculated $K_{O/G}$ with experimental $K_{O/G}$ values. The availability of data for parent PAHs and the lack thereof for their substituted counterparts is expected, mainly because parent "priority" PAHs received most of the attention so far, with the SPAHs becoming subject to investigation only more recently.

Because experimental data are not available for most SPAHs, we also compared the COSMOtherm-predicted values with those obtained by other prediction tools, specifically ppLFERs, with solute descriptors taken either from the UFZ-LSER database[53] (parent PAHs) or predicted with ABSOLV (ACD/Labs, Advanced Chemistry Development, Inc., Toronto, Canada) (SPAHs). ppLFERs for the relevant partition coefficients were obtained from Arp *et al.*[54] for $K_{WIOM/G}$, Wang *et al.*[23] for K_S, Goss[55] for $K_{W/G}$ and Roth *et al.*[51] for $K_{S/G}$. $K_{W/G}$ and $K_{WIOM/G}$ were also predicted using the SPARC (SPARC Performs Automated Reasoning in Chemistry) software and $K_{W/G}$ was predicted using the Estimation Program Interface Suite (EPISuite).

When comparing datasets of properties, we calculated the mean difference (MD) and the mean absolute difference (MAD) between the different sets of data using:

$$\mathrm{MD}_{XY} = \frac{1}{n}\sum\left((K \text{ or } \log K)_X - (K \text{ or } \log K)_Y\right) \quad (7)$$

$$\mathrm{MAD}_{XY} = \frac{1}{n}\sum\left|(K \text{ or } \log K)_X - (K \text{ or } \log K)_Y\right| \quad (8)$$

where X and Y represent the two methods being compared.

2.4 The chemical partitioning space

A chemical partitioning space diagram displays regions of dominant phase distribution within a coordinate system defined by equilibrium phase partitioning coefficients. Substances can be placed on those diagrams based on their partitioning properties under certain prevailing conditions such as temperature, revealing information on their phase distribution behavior at equilibrium. When applied to three phase systems, partitioning space diagrams are two-dimensional. Lei and Wania[38] used chemical space plots to illustrate phase partitioning in warm and cold clouds. Wania *et al.*[33] also used these plots to display the atmospheric phase distribution of organic compounds involved in secondary organic aerosol formation, both in aerosols and in clouds. In both cases, only three phases were considered – gas, water, particles and gas, water, WIOM respectively. In this work, we opted to include the water surface as a possible phase for equilibrium partitioning in the atmosphere, giving a total of four phases. While equilibrium partitioning between four phases requires a three-dimensional space diagram, such plots tend to be difficult to display and digest. Therefore, two separate two-dimensional space plots are employed here; one based on $K_{G/W}$ and $K_{WIOM/G}$ and the other on $K_{G/S}$ (*i.e.* $1/K_{S/G}$) and $K_{WIOM/G}$. The bulk aqueous phase in the first plot is replaced with the water surface phase in the other. The phase dimensions employed in generating those plots are the same as outlined in Section 2.1 above. The SPAHs are placed on either of those plots based on their estimated distribution behavior. An in-depth description of the chemical partitioning space for the atmosphere can be found in Wania *et al.*[33]

3 Results and discussion

3.1 Evaluation of COSMOtherm predictions

All predicted partition coefficients are given in Table S6 in the ESI.† Fig. S1† shows comparisons between COSMOtherm predicted partitioning coefficients, measured partitioning coefficients and predictions obtained with SPARC, ppLFERs, and EPISuite. Calculated MAD values for $K_{W/G}$ are in the range of 0.20 to 0.43, *i.e.* the methods show very similar performance. Most of the $K_{W/G}$ predictions agree quite well with the measured values, with the only significant outlier being the ppLFER value for benzo(*a*)pyrene (Fig. S1a†). Overall, COSMOtherm shows relatively good agreement with the measured data (MD and MAD in Table S2†). Table S2† further shows that ppLFERs do not perform substantially better than COSMOtherm when judged by the comparison with the experimental data for $K_{O/G}$, $K_{S/G}$ and K_S.

For $K_{S/G}$ and K_S, experimental values were available only for naphthalene for comparison. While the values agreed fairly well with the estimated ones, the data are insufficient to make a definite inference about the performance of the prediction in this case. However, other studies have compared experimental data with COSMOtherm predicted $K_{S/G}$[37] and K_S,[23,42] with observations of excellent and moderate agreement, respectively. COSMOtherm predictions for $K_{G/W}$ and $K_{O/G}$ have also been evaluated with experimental data.[56,57] The general trends observed are similar to those in this work (Fig. S1†). Stenzel *et al.*[58] also validated COSMOtherm with experimental data for a large set of multifunctional chemicals in well-defined partitioning systems.

The range of MAD between COSMOtherm and other prediction methods (for $K_{W/G}$), 0.39 to 0.64, though higher than the MAD between COSMOtherm and measured data, still shows reasonable agreement, with EPISuite displaying the least agreement (Fig. S1 and Table S3†). The MAD of the three other coefficients (COSMOtherm *vs.* ppLFER) again shows good agreement, particularly for K_S, 0.07. As mentioned previously, we compared COSMOtherm predicted $K_{WIOM/G}$ values with experimental $K_{O/G}$ values and the agreement between these (0.52) is slightly better than that between COSMOtherm predicted $K_{WIOM/G}$ and $K_{WIOM/G}$ predicted with ppLFER (0.71).

Based on the reasonable agreement with measured numbers, COSMOtherm predictions were deemed suitable to form the basis for the analysis that follows below. They were further judged to be preferable over other prediction methods, because COSMOtherm predictions (i) are possible for all four of the *K*-values required for our analysis, (ii) do not have applicability domains limited by the diversity of an empirical dataset, and (iii) appear to agree at least as well with the empirical evidence as other predictions. However, one should keep in mind that based on the comparison conducted here the *K*-values may have uncertainties on the order of half a log unit.

3.1.1 Gas particle partitioning of SPAHs: predicted *vs.* measured. Few SPAHs have had their gas–particle partitioning behavior measured under ambient conditions. Wei *et al.*,[3] Li *et al.*[17] and Tomaz *et al.*[18] reported the fractional distribution between gas and particle phases for selected PAHs and SPAHs in the atmosphere (Table S4†). The fractional distribution of each of these compounds was calculated using eqn (1) to (4), whereby partition coefficients predicted by COSMOtherm at the temperature of the measurements were used. Also, site-specific estimates of the organic aerosol load (*i.e.* volume of water insoluble organic matter V_{WIOM}) were applied. The fractions in the three condensed phases, Φ_W, Φ_S and Φ_{WIOM}, were summed to estimate the percentage in the particle phase, which is compared with measured values in Fig. S2.†

The level of agreement between the measured and predicted data varies between compounds and environmental conditions. With the exception of some nitro-substituted PAHs and the larger 4 and 5 ringed PAHs, measured data and COSMOtherm data show good agreement; especially for the smaller compounds. If there are discrepancies, the measured fraction in the particle phase generally exceeds the estimated one. It is difficult to attribute such discrepancies, as they are likely within the uncertainty range of both measurements and predictions and also because the possible reasons are numerous. One possible explanation is that SPAH and PAH do not necessarily achieve equilibrium between the gas and particle phases.[10]

3.2 Phase partitioning in aerosols and clouds

Using the COSMOtherm-estimated values and eqn (1) to (4), the degree of partitioning of PAHs and SPAHs to the different phases in aerosols (Fig. 2) and clouds (Fig. 3) was estimated. Varying the particle size (*i.e.* comparing the left and right panels in Fig. 2 and 3) shows the sensitivity of surface adsorption to this parameter.

In aerosols, only gas and WIOM phases are important for the phase distribution of PAHs and SPAHs (Fig. 2). In particular, none of the 68 PAHs and SPAHs partition to any notable extent into the bulk water phase of aerosols (Fig. 2). Water surface sorption is equally unimportant (Fig. 2a), with the exception of 2,7-dihydroxynaphthalene, benz(*a*)anthracene-3,4-dione and benzo(*a*)pyrene-7,8-dione, for which we estimated that approximately 2%, 3% and 8% respectively, sorb to the water surface at equilibrium in the smaller size aerosol (Fig. 2b). All four phases are evident in the plots for clouds (Fig. 3), suggesting that partitioning to bulk water and water surface is important for at least some SPAHs. Polar SPAHs show significant partitioning to the bulk water phase in clouds. In addition, the water surface also appears to be slightly more prominent than in aerosols.

3.2.1 Is the salting-out effect responsible for the lack of aqueous bulk phase partitioning of SPAHs in aerosols? While the bulk water phase was not important for any of the SPAHs in aerosols (Fig. 2), some SPAHs are predicted to dissolve to a significant extent in cloud water (Fig. 3). The question arises whether this is due to the effect of the high salt content assumed in the aerosol scenario. In that scenario, the $K_{W/G}$ value was corrected for the salt effect. The predicted K_S is positive for all 68 compounds, *i.e.* their partitioning is shifted from the bulk water phase to the non-aqueous phases, *i.e.* gas phase, WIOM phase and water surface. We estimate that the salt-effect reduced the $K_{W/G}$ by as much as 200%, indicating that the inorganic salts present in aerosols have the potential to greatly reduce partitioning of SPAHs to the aqueous phase.

However, when comparing partitioning calculations with and without the consideration of the salting out effect (Fig. S3†), the result for only a single substance was sensitive to this change. 2,7-Dihydroxynaphthalene is the only compound partitioning slightly (2%) into the bulk aqueous phase of the aerosol, likely due to its small size and the presence of OH groups, which readily form hydrogen bonds with water molecules. When the salt effect is considered, its partitioning is shifted from the bulk aqueous phase to the gas phase and the WIOM phase.

Generally, the aqueous bulk phase appears not to be a major partitioning phase for SPAHs in aerosols (with or without salting-out), largely a result of the small water volume in aerosols, because in clouds, bulk aqueous phase partitioning is estimated to be important for selected SPAHs. It follows that the salting out effect may only need to be considered when estimating the atmospheric phase partitioning of small SPAHs with highly polar substituents; and can be neglected for other less polar and heavier SPAHs.

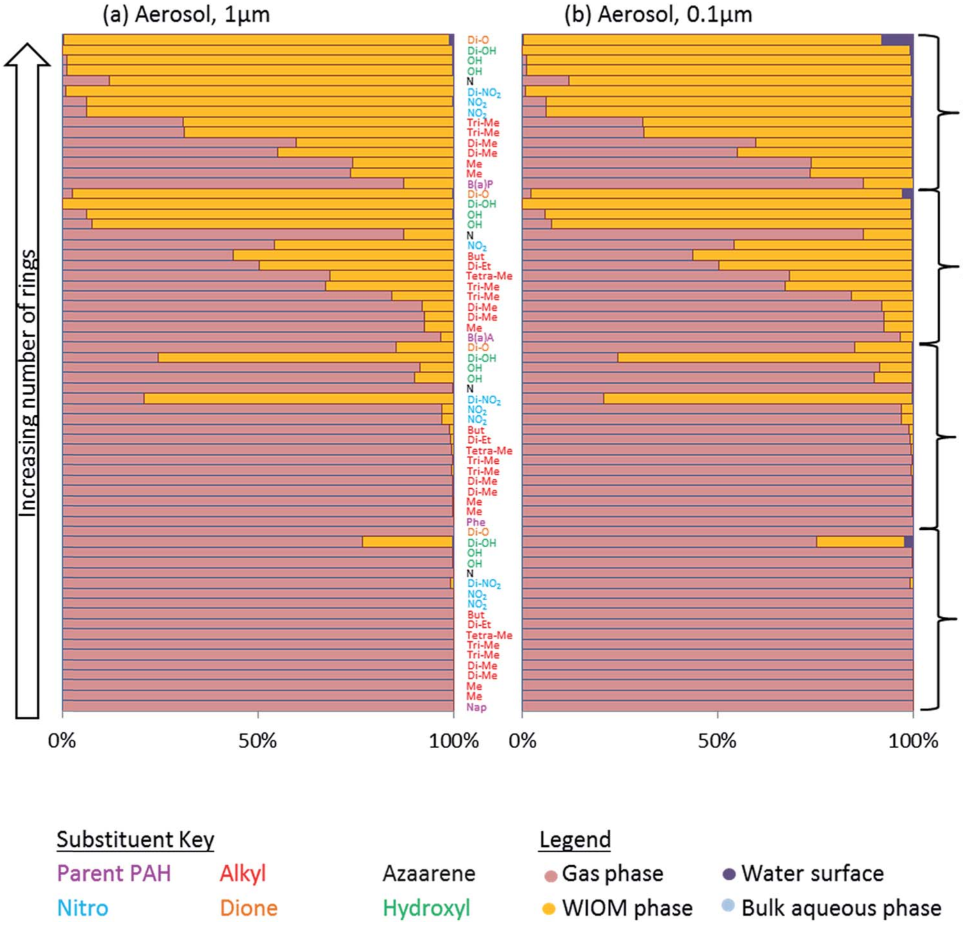

Fig. 2 Partitioning of PAHs and SPAHs in aerosols of different sizes. The total surface area of the aerosol in (a) is 3×10^{-5} m^2 m^{-3} gas; (b) is 3×10^{-4} m^2 m^{-3} gas. The acronyms for different SPAHs are defined in Table S1.†

3.2.2 Adsorption of SPAHs onto the surface of aerosols and cloud droplets. Although water surface sorption does not appear to be a very important process for SPAHs, the results in Fig. 2 and 3 still indicate that the size of the aerosol or cloud droplet determines the extent to which compounds partition to the water surface. These figures also suggest that the water surface is more important in clouds than in aerosols. At first this seems counterintuitive due to the fact that aerosols due to their smaller droplet size have a larger surface area-to-volume ratio than clouds. If water were the only condensed phase present in the atmosphere, the increasing surface area-to-volume ratio with decreasing droplet size would indeed require that compounds that are in the bulk water phase in a cloud shift their distribution to the water surface in an aerosol. However, the atmosphere also contains WIOM, and therefore the water surface-to-WIOM volume ratio also matters.

Simple calculations (Table S5†) show that even though aerosol droplets are smaller (by about three orders of magnitude) and of a larger number than cloud droplets, the total water surface area per volume of air is actually higher in clouds than in aerosols (by about two orders of magnitude) because of the much higher LWC of clouds (higher by more than four orders of magnitude). In other words, the water surface area-to-WIOM volume ratio is often smaller in aerosols than in clouds, and because WIOM is a more important bulk phase than water for most SPAHs, water surface adsorption of SPAHs is more likely to be a notable process in clouds than in aerosols (this suggests that for more water-soluble substances than the SPAHs, *i.e.* substances for which the WIOM phase is not important, the water surface may play a larger role in aerosols than in clouds, because the water surface area-to-water volume ratio in aerosols is more important than the water surface area-to-WIOM volume ratio).

Large organic compounds, even those that are insoluble in water, can move from the WIOM phase onto the water surface, provided the available surface area is large enough (larger than that assumed in this work). The results also indicate that the relative affinity of SPAHs for the water surface or the bulk aqueous phase is dependent on the size of the compound, the nature of the substituent and the size of the respective phases.

3.3 Effect of addition of substituents and rings on the relative affinity of SPAHs for different atmospheric phases

Modifications to the structure of a PAH, be it the addition of a polar or non-polar (alkyl) substituent, or an additional ring, have effects on the partition coefficient of the compound, and

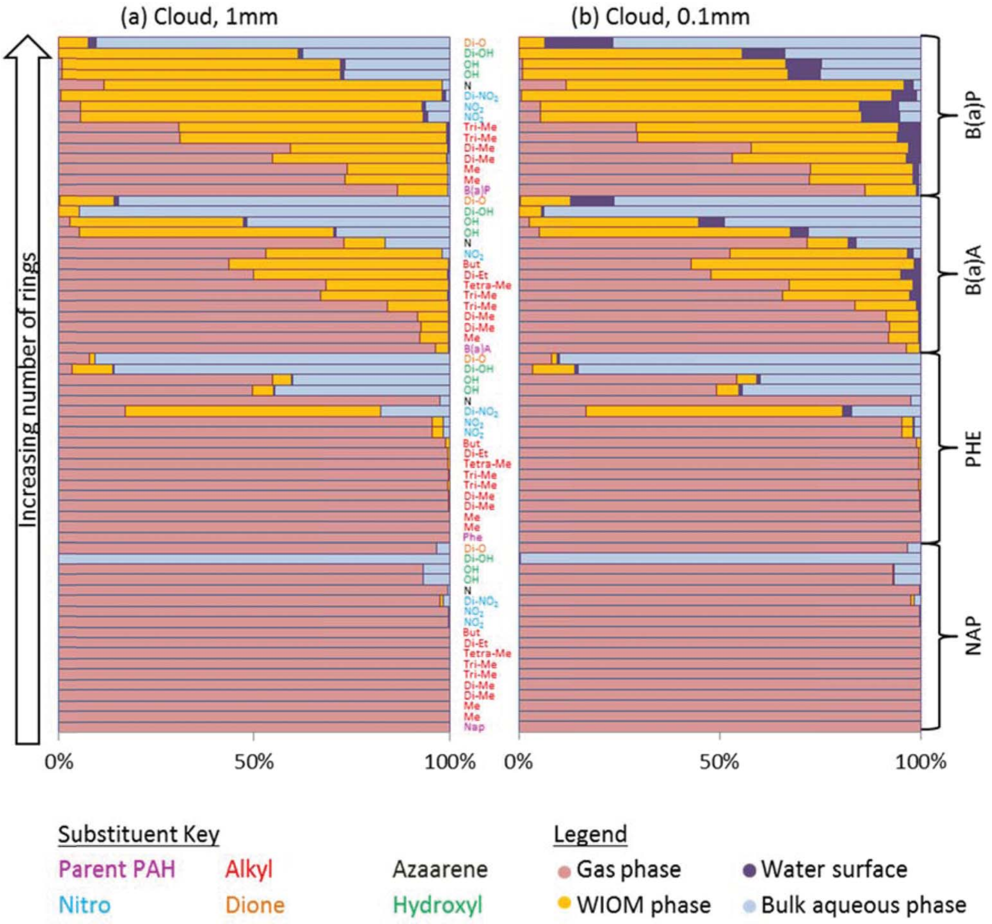

Fig. 3 Partitioning of PAHs and SPAHs in clouds with droplets of different radii. The total surface area of the cloud in (a) is 9×10^{-4} m^2 m^{-3} gas; (b) is 9×10^{-3} m^2 m^{-3} gas. The acronyms for different SPAHs are defined in Table S1.†

correspondingly, on the affinity of the compound for different phases in the environment. Fig. 4 summarizes the average COSMOtherm-predicted changes to $K_{WIOM/G}$, $K_{S/G}$ and $K_{W/G}$ (collectively referred to as $K_{X/G}$) arising from these molecular modifications. Generally, the addition of polar functional groups elicits the largest increases in the $K_{X/G}$-values, with hydroxyl and dione functionalities showing the most dramatic increase in the affinities of PAHs to the three condensed phases, with that increase being larger for the bulk water phase than the water surface, which in turn is larger than for the WIOM phase. In Fig. 4, it appears that the addition of a dione functionality elicits the largest increase. However, upon normalization to the mass change associated with a structural change (Fig. S4†), it is seen that the hydroxyl group actually causes a slightly higher increase than the dione. A nitro-group has less of an effect, especially when normalized to the mass change, indicating similar incremental increases in the $K_{X/G}$ values through the addition of nitro-groups and additional aromatic rings.

The addition of alkyl substituents, additional rings and nitro-groups increases $K_{WIOM/G}$ and $K_{S/G}$ values by almost the same extent, *i.e.* does not change the relative affinity of a SPAH for the WIOM phase and the water surface. On the other hand, alkyl addition does not change the $K_{W/G}$ very much at all, presumably because a decrease in water solubility is matched almost exactly by a decrease in volatility. The replacement of a carbon with a nitrogen within the aromatic ring system (*i.e.* the formation of an azaarene) has a surprisingly large effect on

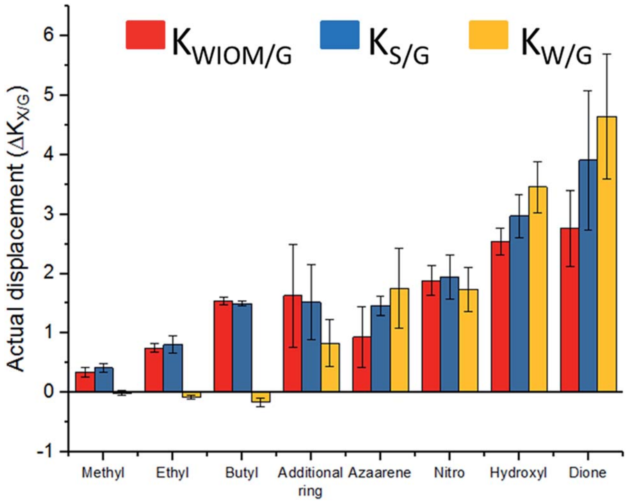

Fig. 4 Average change in the COSMOtherm-predicted values of $K_{WIOM/G}$, $K_{S/G}$ and $K_{W/G}$ upon addition of different functional groups to polycyclic aromatic hydrocarbons.

the partitioning properties of a PAH, especially when normalized to the very small mass change associated with this replacement (Fig. S4†). Overall, the COSMOtherm predictions indicate that alkyl groups and additional rings cause an increase in the affinity of a PAH for the water surface and the WIOM phase at the expense of the aqueous bulk phase, while the effect of the addition of hydroxyl and carbonyl functionalities is larger and in the opposite direction, *i.e.* favors the aqueous bulk phase and to a lesser extent the water surface over the WIOM phase.

3.4 Displaying SPAHs on the chemical partitioning space for aerosols and clouds

The error bars in Fig. 4 indicate that there is some variability in the incremental change in $K_{X/G}$ depending on which PAHs and on which position on a PAH the structural change takes place. The changes in the partitioning properties arising from structural modifications of individual compounds are shown in Fig. S5 in the ESI†. Arrows in that figure indicate the displacement in the chemical partitioning space caused by structural modifications: the starting point of an arrow indicates the position of the parent PAH while the arrows show the displacement resulting from the addition of a particular substituent.

Three partition coefficients are required to fully characterize the distribution between the four phases we consider in our analysis. Instead of using a three-dimensional plot that is difficult to display and digest, Fig. S5† consists of four two-dimensional plots. In these plots a displacement with a slope of -1 indicates a change in partitioning properties that does not lead to a shift in the affinity of a compound from one condensed phase to another. A displacement with a slope steeper (less steep) than -1 indicates that affinity is shifted to the condensed phase represented by the partitioning coefficient on the *y*-axis (*x*-axis).

Plots of the type displayed in Fig. S5† can only serve to indicate the changes in the equilibrium phase distribution of a compound caused by molecular structural modifications when complemented by information on the dimension of the phases in the atmosphere.[33] Since the bulk aqueous phase and the water surface were found not to be important for any SPAHs in aerosols (Fig. 2), space plots based either on $K_{S/G}$ and $K_{WIOM/G}$ (Fig. 5A) or $K_{W/G}$ and $K_{WIOM/G}$ (Fig. 5B) are suitable for displaying the equilibrium phase distribution in aerosols.

In clouds, SPAHs are estimated to partition to all four phases to some extent (Fig. 3). Fig. 6A shows a plot based on $K_{S/G}$ and $K_{WIOM/G}$ and can accommodate substances for which the aqueous bulk phase plays a negligible role, while Fig. 6B is based on $K_{W/G}$ and $K_{WIOM/G}$, *i.e.* is appropriate for substances that do not appreciably partition to the water surface. If a substance is predicted to partition less than 5% to the water surface, it is placed in Fig. 6A. If it partitions less than 5% to the bulk aqueous phase, it is placed in Fig. 6B. Because hydroxyl and nitro-PAHs partition more than 5% to all four phases, they cannot be placed on either of these plots. In a cloud, the water surface is a minor partitioning medium for the majority of SPAHs, and they therefore are placed in Fig. 6A.

3.4.1 Influence of molecular structural attributes on phase partitioning in aerosols. Fig. 5A and B are similar to Fig. S5D and S5A† except that in this case, a background showing the phase distribution in an aerosol is included (assuming

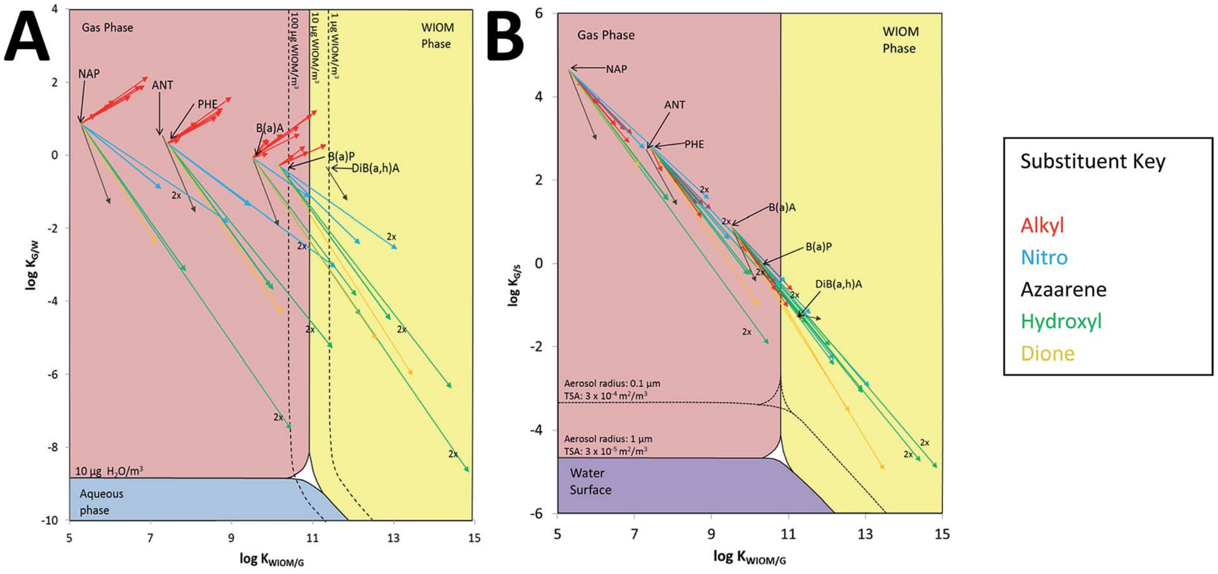

Fig. 5 Chemical partitioning space showing the partitioning of PAHs and SPAHs within an atmospheric aerosol. The red, yellow, blue and purple colors represent the gas phase, WIOM phase, bulk water phase and water surface, respectively. Dashed lines in (A) indicate the 50% threshold for various loadings of WIOM, while those in (B) show a scenario with smaller particles. The starting point of the arrows indicates the position of the parent PAH (NAP: naphthalene, ANT: anthracene, PHE: phenanthrene, B(*a*)A: benz(*a*)anthracene, B(*a*)P: benzo(*a*)pyrene, DiB(*a*,*h*)A: dibenz(*a*,*h*)anthracene) while the arrows show the displacement resulting from the addition of a particular substituent. Arrows labelled with 2× indicate diols (green) and di-nitro (blue) substituents.

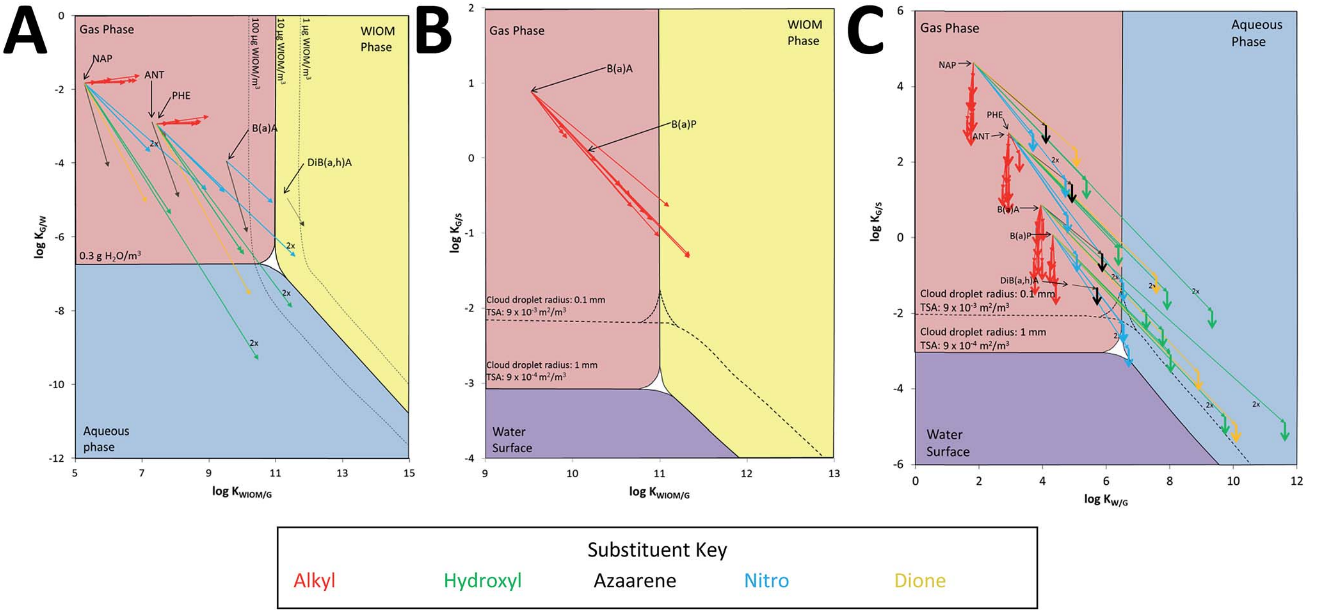

Fig. 6 Chemical partitioning space showing the partitioning of PAHs and SPAHs within a cloud that either has separate aqueous and WIOM phases (A and B) or only a single aqueous phase (C). The red, yellow, blue and purple colors represent the gas phase, WIOM phase, bulk aqueous phase and water surface, respectively. Dashed lines in (A) indicate the 50% threshold for various loadings of WIOM, while those in (B) and (C) show a scenario with smaller droplets. The starting point of the arrows indicates the position of the parent PAH (NAP: naphthalene, ANT: anthracene, PHE: phenanthrene, B(*a*)A: benz(*a*)anthracene, B(*a*)P: benzo(*a*)pyrene, DiB(*a*,*h*)A: dibenz(*a*,*h*)anthracene) while the arrows show the displacement resulting from the addition of a particular substituent. Arrows labelled with 2× indicate diols (green) and di-nitro (blue) substituents. The bold arrows in C show the change in partitioning caused by the presence of an organic film on the droplet surface.

10 μg m^{-3} of WIOM, 10 μg m^{-3} of liquid water and an average droplet radius of 1 μm). Fig. 5 indicates that at 25 °C, all substituted naphthalenes are estimated to be entirely in the gas phase. In the case of phenanthrene, two highly polar substituents (*e.g.* two nitro or two hydroxyl groups) are required to shift phase distribution from the gas to the WIOM phase, while a substituted benzo(*a*)pyrene will almost inevitably be in the condensed phase under the assumed atmospheric conditions.

The diagonal stripe with most of the arrows in Fig. 5B is nearly parallel to the line separating the purple and yellow regions, which indicates the 50% threshold for partitioning between the water surface and the WIOM phase. The arrows are placed well above the threshold, because $V_{\mathrm{WIOM}}K_{\mathrm{WIOM/G}}$ is on average larger than $AK_{\mathrm{G/S}}$ by approximately three orders of magnitude, making WIOM the dominant condensed phase. The addition of azaarene, dione and hydroxyl substituents to PAHs increases the affinity for the water surface slightly more than the affinity for WIOM. However, this is of little consequence, as WIOM remains the dominant condensed phase. Similarly, in Fig. 5A, while substitution leads to more pronounced changes in the relative affinity of a PAH for WIOM and aqueous bulk phases (*i.e.* the arrows point in different directions), these changes have little impact on phase distribution in aerosols, because $V_{\mathrm{WIOM}}K_{\mathrm{WIOM/G}}$ is larger than $V_{\mathrm{W}}K_{\mathrm{W/G}}$ and WIOM therefore dominates.

3.4.2 Influence of molecular structural attributes on phase partitioning in clouds. The plots in Fig. 6A and B show the phase distribution of SPAHs in a cloud that has separate aqueous and WIOM phases. Not all 68 compounds are included in these plots, for reasons mentioned in Section 3.4. While the displacement of the SPAHs in Fig. 6 is almost identical to Fig. 5, differences arise because of different phase sizes and the salting out effect. Clouds have much higher liquid water content (assumed to be 0.3 g m^{-3}) than aerosols, and this translates to a larger area indicating dominant partitioning into the bulk aqueous phase. SPAHs with two polar substituents (*e.g.* diols of naphthalene and phenanthrene and the dione of phenanthrene) are predicted to partition to a large extent into the aqueous phase (Fig. 6A). Comparing Fig. 6A and 5A shows that some SPAHs, which remain in the gas phase in an aerosol, are more likely to be in the bulk aqueous phase under cloud conditions.

In Fig. 6B, which shows the preference of some SPAHs for the water surface and the WIOM phase, none of the displayed arrows crosses into the area indicating notable adsorption to the water surface because the total surface area per unit volume of a cloud droplet is still not large enough to compete with absorption into the WIOM phase. However, as is seen from the comparison of Fig. 3a and b, a decrease in the radius of a cloud droplet tends to slightly favor water surface adsorption.

Because of the large LWC in cloud droplets it is possible that all of the non-gaseous organic compounds dissolve in the aqueous phase and no separate WIOM phase forms. The resulting 3-phase system comprising gas, water surface, and bulk aqueous phase is depicted in Fig. 6C. In the absence of a WIOM phase, polar SPAHs partition mostly into the bulk aqueous phase, while non-polar compounds are mostly in the gas phase. The affinity for the water surface clearly increases with molecular size.

It is also possible that non-soluble organic compounds form an organic film on the cloud droplet surface rather than dissolving in the aqueous phase or forming a distinct WIOM phase. Studies indicated that the presence of organic films can enhance the sorption of organic compounds to the water surface.[59,60] To account for this effect, we increased the $K_{S/G}$ for all SPAHs by a factor of 3, based on the observed difference in the adsorption of PAHs to pure and organic-coated water surfaces.[59] The displacement in the partitioning space caused by enhanced surface partitioning is indicated by the bold, short, downward pointing arrows in Fig. 6C. The figure indicates that for the larger SPAHs (4 and 5 rings) with hydroxyl, nitro, and carbonyl substituents the effect of an organic coating on surface adsorption can indeed make a difference to the importance of the droplet surface relative to the bulk aqueous phase of a cloud, especially if the cloud droplets are relatively small.

The advantage of plotting the phase distribution behavior of the SPAHs in a partitioning space as in Fig. 5 and 6 is that the change in the phase distribution occurring as a result of a molecular modification can be compared with the changes caused by other factors.[33] For example, in Fig. 5A and 6A, the broken lines indicate how atmospheric phase distribution would change if the organic aerosol load were either higher or lower than the default 10 $\mu g\ m^{-3}$, while in Fig. 5B and 6B and C, similar lines show the sensitivity of the results to the droplet radius. Other factors that could be similarly explored in such plots are the effects of temperature or parameter uncertainty.[33] The effects of parameter uncertainties and assumptions regarding parameters such as phase volume and particle size are more prominent for some compounds than others. For example, for a compound like naphthalene, which is placed at the extreme left of the gas phase-dominated area in Fig. 5A and B and 6A and C, uncertainties and assumptions will likely not have an effect significant enough to result in a phase change. A compound like benz(*a*)anthracene, which falls close to the boundary between two phases, is more likely to change phases as a result of uncertainty.

4 Conclusion

We have demonstrated that the quantum-chemistry based COSMOtherm software provides an effective tool for the comprehensive assessment of the gas–particle partitioning characteristics of organic compounds, if only their molecular structure is known. In contrast to other methods used for the estimation of gas–particle partitioning, neither saturation liquid vapor pressure nor $K_{O/G}$ needs to be known or estimated and neither is it necessary to rely on regressions on empirical data that typically have limited domains of applicability.

The chemical equilibrium partitioning space is used here to explore the impact of the addition of functional groups and aromatic rings on the phase distribution behavior of PAHs in the atmosphere. All additions were found to shift the affinity of a PAH from the gas to the WIOM phase, with polar functional groups having a much larger impact than alkyl substituents. The particular position of a substituent has little or no effect. Only the addition of two polar functional groups to relatively small PAHs with two or three rings increases the affinity for the aqueous phase sufficiently for it to become the dominant phase under the conditions prevailing in clouds.

The results from this study thus generally indicate that the simplifications normally employed when predicting the gas–particle partitioning of SPAHs in aerosols are mostly valid. The salting-out effect is predicted to have a negligible influence on the phase partitioning of these compounds in aerosols. Furthermore, since neither the bulk aqueous phase nor the water surface plays a notable role in the aerosol phase partitioning of SPAHs, it also appears valid to assume aerosols to be composed of a single bulk organic phase. However, when estimating phase partitioning in clouds, it may be misleading not to consider all phases for PAHs and SPAHs.

We should note that the presented approach has a number of limitations. Notably, no consideration is given to sorption of SPAHs to black carbon.[20,22] While soot has potentially a large uptake capacity for SPAHs, the availability of that capacity in ambient aerosols is doubtful, as the soot may be coated with salts and organic matter.[61,62] Note also that earlier studies indicating the importance of soot[20] have been based on flawed adsorption constants.[63]

With the exception of the calculations performed in Section 3.1.1, the presented partitioning equilibria are for 25 °C, even though ambient atmospheric temperatures are varying widely and gas phase/condensed phase partitioning equilibria are highly temperature dependent. While COSMOtherm is capable of predicting solvation properties at other temperatures, its performance with respect to predicting the temperature dependence of atmospherically relevant partitioning equilibria still needs to be established.

Acknowledgements

Funding was provided by Environment and Climate Change Canada and a TD Canada Trust Scholarship.

References

1 H. Yu, *J. Environ. Sci. Health, Part C: Environ. Carcinog. Ecotoxicol. Rev.*, 2002, **20**, 149–183.

2 C. Achten and J. T. Andersson, *Polycyclic Aromat. Compd.*, 2015, **35**, 177–186.

3 C. Wei, Y. Han, B. A. M. Bandowe, J. Cao, R.-J. Huang, H. Ni, J. Tian and W. Wilcke, *Sci. Total Environ.*, 2015, **505**, 814–822.

4 M. S. Shailaja, R. Rajamanickam and S. Wahidulla, *Toxicol. Sci.*, 2006, **91**, 440–447.

5 S. Lundstedt, P. A. White, C. L. Lemieux, K. D. Lynes, I. B. Lambert, L. Öberg, P. Haglund and M. Tysklind, *Ambio*, 2007, **36**, 475–485.

6 K. Misaki, T. Takamura-Enya, H. Ogawa, K. Takamori and M. Yanagida, *Mutagenesis*, 2016, **31**, 205–213.

7 P. Lin, P. K. Aiona, Y. Li, M. Shiraiwa, J. Laskin, S. A. Nizkorodov and A. Laskin, *Environ. Sci. Technol.*, 2016, **50**, 11815–11824.

8 T. F. Bidleman, *Environ. Sci. Technol.*, 1988, **22**, 361–367.

9 S. Zhou, A. K. Y. Lee, R. D. McWhinney and J. P. D. Abbatt, *J. Phys. Chem. A*, 2012, **116**, 7050–7056.

10 S. Zhou, M. Shiraiwa, R. D. McWhinney, U. Pöschl and J. P. D. Abbatt, *Faraday Discuss.*, 2013, **165**, 391–406.

11 B. Huang, M. Liu, X. Bi, C. Chaemfa, Z. Ren, X. Wang, G. Sheng and J. Fu, *Atmos. Pollut. Res.*, 2014, **5**, 210–218.

12 J. F. Pankow and T. F. Bidleman, *Atmos. Environ., Part A*, 1991, **25**, 2241–2249.

13 G. P. Klein, E. M. Hodge, M. L. Diamond, A. Yip, T. Dann, G. Stern, M. S. Denison and P. A. Harper, *Environ. Health Perspect.*, 2005, **114**, 697–703.

14 E. O. Gaga and A. Ari, *Atmos. Res.*, 2011, **99**, 207–216.

15 P. Fernández, J. O. Grimalt and R. M. Vilanova, *Environ. Sci. Technol.*, 2002, **36**, 1162–1168.

16 I. E. Sitaras, E. B. Bakeas and P. A. Siskos, *Sci. Total Environ.*, 2004, **327**, 249–264.

17 W. Li, G. Shen, C. Yuan, C. Wang, H. Shen, H. Jiang, Y. Zhang, Y. Chen, S. Su, N. Lin and S. Tao, *Atmos. Res.*, 2016, **172–173**, 66–73.

18 S. Tomaz, P. Shahpoury, J.-L. Jaffrezo, G. Lammel, E. Perraudin, E. Villenave and A. Albinet, *Sci. Total Environ.*, 2016, **565**, 1071–1083.

19 J. F. Pankow, *Atmos. Environ.*, 1987, **21**, 2275–2283.

20 J. Dachs and S. J. Eisenreich, *Environ. Sci. Technol.*, 2000, **34**, 3690–3697.

21 A. Finizio, D. Mackay, T. Bidleman and T. Harner, *Atmos. Environ.*, 1997, **31**, 2289–2296.

22 R. Lohmann and G. Lammel, *Environ. Sci. Technol.*, 2004, **38**, 3793–3803.

23 C. Wang, Y. D. Lei, S. Endo and F. Wania, *Environ. Sci. Technol.*, 2014, **48**, 13238–13245.

24 L. Renbaum-Wolff, M. Song, C. Marcolli, Y. Zhang, P. F. Liu, J. W. Grayson, F. M. Geiger, S. T. Martin and A. K. Bertram, *Atmos. Chem. Phys.*, 2016, **16**, 7969–7979.

25 D. J. Stewart, C. Cai, J. Nayler, T. C. Preston, J. P. Reid, U. K. Krieger, C. Marcolli and Y. H. Zhang, *J. Phys. Chem. A*, 2015, **119**, 4177–4190.

26 Y. You, L. Renbaum-Wolff, M. Carreras-Sospedra, S. J. Hanna, N. Hiranuma, S. Kamal, M. L. Smith, X. Zhang, R. J. Weber, J. E. Shilling, D. Dabdub, S. T. Martin and A. K. Bertram, *Proc. Natl. Acad. Sci. U. S. A.*, 2012, **109**, 13188–13193.

27 Y. You, M. L. Smith, M. Song, S. T. Martin and A. K. Bertram, *Int. Rev. Phys. Chem.*, 2014, **33**, 43–77.

28 L. Renbaum-Wolff, J. W. Grayson, A. P. Bateman, M. Kuwata, M. Sellier, B. J. Murray, J. E. Shilling, S. T. Martin and A. K. Bertram, *Proc. Natl. Acad. Sci. U. S. A.*, 2013, **110**, 8014–8019.

29 M. Shiraiwa, A. Zuend, A. K. Bertram and J. H. Seinfeld, *Phys. Chem. Chem. Phys.*, 2013, **15**, 11441–11453.

30 A. Albinet, E. Leoz-Garziandia, H. Budzinski, E. Villenave and J.-L. Jaffrezo, *Atmos. Environ.*, 2008, **42**, 43–54.

31 S. Endo and K.-U. Goss, *Environ. Sci. Technol.*, 2014, **48**, 12477–12491.

32 H. P. H. Arp and K.-U. Goss, *Environ. Sci. Technol.*, 2009, **43**, 1923–1929.

33 F. Wania, Y. D. Lei, C. Wang, J. P. D. Abbatt and K.-U. Goss, *Atmos. Chem. Phys.*, 2015, **15**, 3395–3412.

34 H. Herrmann, T. Schaefer, A. Tilgner, S. A. Styler, C. Weller, M. Teich and T. Otto, *Chem. Rev.*, 2015, **115**, 4259–4334.

35 C. Wang, K.-U. Goss, Y. D. Lei, J. P. D. Abbatt and F. Wania, *Environ. Sci. Technol.*, 2015, **49**, 8585–8594.

36 A. Zuend and J. H. Seinfeld, *Atmos. Chem. Phys.*, 2012, **12**, 3857–3882.

37 K.-U. Goss, *J. Phys. Chem. A*, 2009, **113**, 12256–12259.

38 Y. D. Lei and F. Wania, *Atmos. Environ.*, 2004, **38**, 3557–3571.

39 S. H. Cheng, L. X. Yang, X. H. Zhou, L. K. Xue, X. M. Gao, Y. Zhou and W. X. Wang, *Atmos. Environ.*, 2011, **45**, 4631–4640.

40 J. E. Shilling, Q. Chen, S. M. King, T. Rosenoern, J. H. Kroll, D. R. Worsnop, P. F. DeCarlo, A. C. Aiken, D. Sueper, J. L. Jimenez and S. T. Martin, *Atmos. Chem. Phys.*, 2009, **9**, 771–782.

41 R. P. Schwarzenbach, P. M. Gschwend and D. M. Imboden, *Environmental Organic Chemistry*, John Wiley & Sons, New York, United States, 2nd edn, 2003.

42 S. Endo, A. Pfennigsdorff and K.-U. Goss, *Environ. Sci. Technol.*, 2012, **46**, 1496–1503.

43 A. Klamt, *Wiley Interdiscip. Rev.: Comput. Mol. Sci.*, 2011, **1**, 699–709.

44 F. Eckert and A. Klamt, *AIChE J.*, 2002, **48**, 369–385.

45 A. Klamt, *Fluid Phase Equilib.*, 2016, **407**, 152–158.

46 D. M. Lowe, P. T. Corbett, P. Murray-Rust and R. C. Glen, *J. Chem. Inf. Model.*, 2011, **51**, 739–753.

47 N. M. O'Boyle, M. Banck, C. A. James, C. Morley, T. Vandermeersch and G. R. Hutchison, *J. Cheminf.*, 2011, **3**, 33.

48 D. Mackay, W. Y. Shiu, M. Kuo-Ching and S. C. Lee, *Handbook of Physical–Chemical Properties and Environmental Fate for Organic Chemicals: Volume 1: Introduction and Hydrocarbons*, Lewis Publishers, US, Boca Raton, FL, 2nd edn, 2006.

49 Y.-G. Ma, Y. D. Lei, H. Xiao, F. Wania and W.-H. Wang, *J. Chem. Eng. Data*, 2010, **55**, 819–825.

50 W.-H. Xie, W.-Y. Shiu and D. Mackay, *Mar. Environ. Res.*, 1997, **44**, 429–444.

51 C. M. Roth, K.-U. Goss and R. P. Schwarzenbach, *J. Colloid Interface Sci.*, 2002, **252**, 21–30.

52 J. Radonic, M. Vojinovic-Miloradov, M. Turk-Sekulic, J. Kiurski, M. Djogo and D. Milovanovic, *J. Serb. Chem. Soc.*, 2011, **76**, 447–458.

53 S. Endo, T. N. Brown, N. Watanabe, N. Ulrich, G. Bronner, M. H. Abraham and K.-U. Goss, *UFZ-LSER database v. 3.1*, Helmholtz Centre for Environmental Research-UFZ, Leipzig, Germany, 2015, http://www.ufz.de/lserd.

54 H. P. H. Arp, R. P. Schwarzenbach and K.-U. Goss, *Environ. Sci. Technol.*, 2008, **42**, 5951–5957.

55 K.-U. Goss, *Chemosphere*, 2006, **64**, 1369–1374.

56 J. M. Parnis, D. Mackay and T. Harner, *Atmos. Environ.*, 2015, **110**, 27–35.

57 H. P. H. Arp, C. Niederer and K.-U. Goss, *Environ. Sci. Technol.*, 2006, **40**, 7298–7304.

58 A. Stenzel, K.-U. Goss and S. Endo, *Environ. Toxicol. Chem.*, 2014, **33**, 1537–1543.

59 B. T. Mmereki, S. R. Chaudhuri and D. J. Donaldson, *J. Phys. Chem. A*, 2003, **107**, 2264–2269.

60 D. J. Donaldson, B. T. Mmereki, S. R. Chaudhuri, S. Handley and M. Oh, *Faraday Discuss.*, 2005, **130**, 227–239.

61 K.-U. Goss and S. J. Eisenreich, *Atmos. Environ.*, 1997, **31**, 2827–2834.

62 C. M. Roth, K.-U. Goss and R. P. Schwarzenbach, *Environ. Sci. Technol.*, 2005, **39**, 6632–6637.

63 K.-U. Goss, *Environ. Sci. Technol.*, 2004, **38**, 1622–1623.